Acta Crystallographica Section B
Structural Science
ISSN 0108-7681

The *not so* simple cubic structure of $PbZr_{1-x}Ti_xO_3$ (PZT): complex local structural effects in perovskites

Nan Zhang,[a]‡ Hiroko Yokota,[b] A. M. Glazer[a]* and P. A. Thomas[c]

[a]Department of Physics, Oxford University, Parks Rd, Oxford OX1 3PU, England, [b]Graduate School of Science, Department of Physics, Chiba University, Japan, and [c]Physics Department, Warwick University, Coventry CV4 7AL, England

‡ Current address: Department of Chemistry, Simon Fraser University Burnaby, BC, V5A 1S6, Canada.

Correspondence e-mail: glazer@physics.ox.ac.uk

Received 20 August 2011
Accepted 25 September 2011

High-resolution neutron diffraction on the important piezoelectric lead zirconate titanate (PZT) has found that oxygen disorder exists well into the cubic phase. This unexpected result shows that within this phase there persists a remnant of the tilted oxygen octahedra present within the room-temperature ferroelectric phase. The result is that the cubic phase, far from having a simple crystal structure, exhibits a more complex local structure than had hitherto been thought.

1. Introduction

Traditionally, studies of the crystal structures of the cubic (aristotype) phase of perovskites have largely been neglected. This is because the presumed ordered structure has all atoms at special positions fixed by the crystallographic symmetry, and so there are very few structural parameters to vary. Therefore, most studies of perovskite structures, particularly those addressing technologically important materials such as PZT, where piezoelectric properties are found in lower-symmetry phases, have confined themselves simply to confirming that a high-temperature cubic phase exists. Accordingly, little attention has been paid to the details of local structure – and especially the role of disorder – in the cubic phase. We have shown, for the first time, the existence of significant oxygen octahedral disorder persisting within this phase. As ferroelectric and piezoelectric properties in low-symmetry perovskite oxides are critically dependent on the nature of octahedral distortions and tilts relative to the aristotype, the proper appreciation of the structural details of the cubic phase is paramount for the understanding of structure–property relationships.

The solid solution of lead titanate ($PbTiO_3$) and lead zirconate ($PbZrO_3$), $PbZr_{1-x}Ti_xO_3$ (PZT), has been under discussion for many years. It displays a complicated temperature–composition phase diagram (Jaffe *et al.*, 1971), including the so-called morphotropic phase boundary (MPB) at $x \simeq 0.48$, between rhombohedral and tetragonal phases, around which it shows its highest piezoelectric performance.

On the very high Zr-rich side, there is an approximately temperature-independent phase boundary separating the $PbZrO_3$ phase, space group *Pbam*, and the rhombohedral room-temperature *R*3*c* and high-temperature *R*3*m* phases. The *R*3*c* phase is described by cation displacements along [111] coupled with oxygen octahedral tilting described in the Glazer (1972) notation by $a^-a^-a^-$. In the *R*3*m* phase the tilting is lost but the cation displacements remain. Previous work (Clarke & Glazer, 1974; Whatmore *et al.*, 1978) showed that along the Curie temperature line, where PZT becomes cubic, there is a crossover from first- to second-order behaviour with

increasing Zr content in this region, and a tricritical point close to $x = 0.06$.

Glazer *et al.* (1978) and Corker *et al.* (1998) found that, in refinement of the rhombohedral phase using neutron diffraction data, the Pb atom showed a pronounced disc-shaped anisotropic displacement ellipsoid. Furthermore, Corker *et al.* showed that this could be explained by displacing the Pb atoms away from the rhombohedral threefold axes to create locally monoclinic structures that averaged out to form an overall rhombohedral symmetry.

The MPB is known to separate the Ti-rich tetragonal ($P4mm$) and Zr-rich rhombohedral ($R3c$/$R3m$) phases, which are not group–subgroup related. Noheda *et al.* (1999) proposed an intermediate monoclinic phase whose space group (Cm) is a subgroup of both $R3c$ ($R3m$) and $P4mm$, and thus can act as a 'bridging' phase. Glazer *et al.* (2004) subsequently demonstrated that this monoclinic phase can be formed as a long-range structure by increasing the correlation range of the short-range monoclinic structures suggested by the work of Corker *et al.* as the Ti content increases. In addition, electron-diffraction studies showed structured diffuse scattering across the whole composition range, which was later interpreted by Welberry *et al.* (2010) in terms of short-range correlations of the Pb displacements along ⟨111⟩ directions.

Kuroiwa *et al.* (2005) carried out high-energy synchrotron-radiation powder diffraction experiments in the cubic phase, and noted that in profile fits of $h + k + l$ = odd reflections, the calculated intensities were lower than the observed intensities, while for $h + k + l$ = even reflections they were higher. They explained this by suggesting that the Pb atoms were disordered by being displaced from their high-symmetry positions in the ideal cubic structure. In their model the Pb atoms are shifted along ⟨111⟩ directions for Zr-rich PZT and along ⟨110⟩ directions for Ti-rich compositions. In the case of pure $PbZrO_3$ Aoyagi *et al.* (2002) suggested ⟨110⟩ displacements.

More recently, we have carried out a series of high-resolution time-of-flight neutron diffraction experiments for PZT in the Zr-rich region at 300 K and found that the phases are more complicated than thought hitherto. The best fits by the Rietveld method were obtained with mixed phases of rhombohedral $R3c$ and monoclinic Cm symmetry (Yokota *et al.*, 2009). Further time-of-flight neutron diffraction studies of PZT ceramics in the MPB region at several temperatures suggests that the monoclinic phase exists over the whole region below the Curie temperature so that there are mixtures of rhombohedral and monoclinic symmetry on the Zr-rich side, tetragonal and monoclinic on the Ti-rich side, and three phases coexisting in the MPB region (Zhang *et al.*, 2011).

Apart from the study by Kuroiwa *et al.*, there has been almost no detailed structural work carried out on cubic phases of perovskites, presumably because one would not normally expect anything of interest. Recognizing this oversight, we undertook a high-resolution neutron diffraction study of the cubic phase of PZT to compare with the X-ray diffraction study of Kuroiwa *et al*. Furthermore, neutron diffraction is sensitive to oxygen positions, and so far little attention has been paid to possible oxygen disorder in PZT. We were surprised to discover that at all compositions oxygen disorder persists even into the cubic phase. We contend that the presence of disorder of the oxygen octahedral tilts correlates strongly with the long-range tilting observed in the low-temperature rhombohedral structure, and is therefore highly relevant to our understanding of the origin of the room-temperature piezoelectric properties.

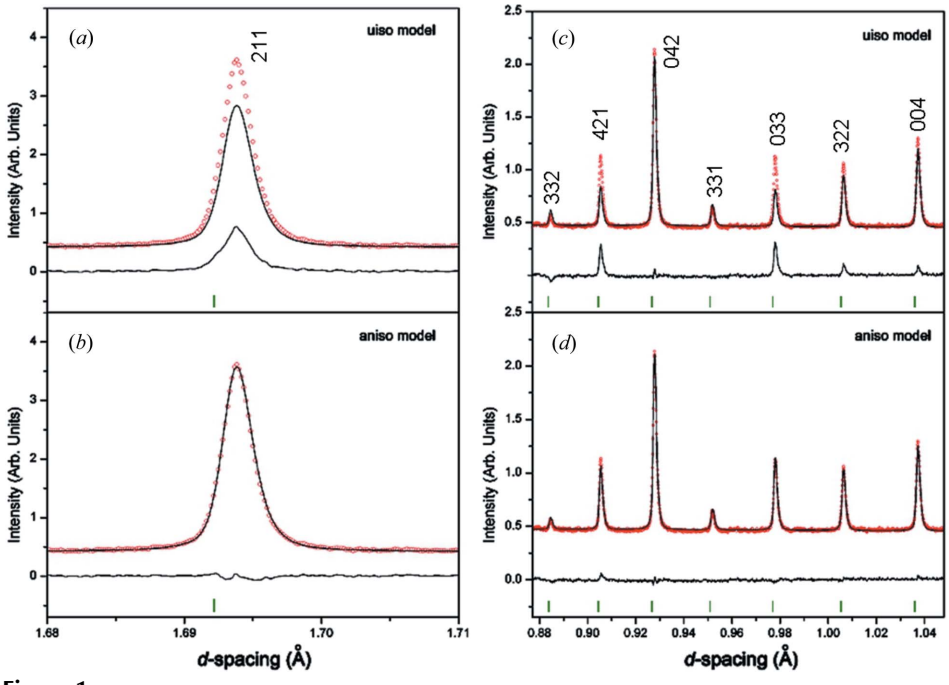

Figure 1
Typical examples of refined profiles for PZT-0.1 at 623 K. The red circles are the observed data and the black line is the calculated pattern. The peak positions are marked by green ticks. (*a*) and (*c*) $Pm\bar{3}m$ model with isotropic displacement parameters; (*b*) and (*d*) $Pm\bar{3}m$ model with anisotropic displacement parameters.

2. Experiment

Ceramic samples were prepared by the conventional mixed-oxide method. The details of sample preparation conditions can be found in the paper by Yokota *et al.* (2009). All the samples were checked at 300 K for the presence of secondary phases and their quality using a Panalytical X'PERT powder diffractometer fitted with an incident-beam Johannssen-cut focusing monochromator to isolate the Cu $K\alpha_1$ line.

The neutron powder diffraction measurements were performed at

Table 1
Values of structural parameters and *R*-factors obtained in Rietveld refinement for isotropic and anisotropic models.

			Isotropic model U_{iso} (Å^2)			Anisotropic model U_{aniso} (Å^2)			
x	T (K)	a (Å)	Pb(U)	Zr/Ti(U)	O(U)	Pb(U)	Zr/Ti(U)	O(U^{11})	O(U^{33})
0	523	4.15972 (1)	0.0559 (3)	0.0074 (2)	0.0399 (3)	0.0583 (2)	0.0111 (1)	0.0670 (2)	0.0088 (2)
	573	4.16130 (1)	0.0577 (3)	0.0080 (2)	0.0400 (3)	0.0598 (2)	0.0116 (1)	0.0663 (2)	0.0093 (2)
0.05	513	4.15212 (2)	0.0600 (5)	0.0091 (3)	0.0406 (4)	0.0609 (3)	0.0129 (2)	0.0632 (4)	0.0118 (4)
	573	4.15378 (2)	0.0600 (5)	0.0095 (3)	0.0398 (3)	0.0612 (3)	0.0133 (2)	0.0630 (3)	0.0105 (3)
	673	4.15704 (1)	0.0628 (5)	0.0108 (3)	0.0404 (3)	0.0641 (3)	0.0147 (2)	0.0638 (3)	0.0114 (3)
0.1	563	4.14337 (1)	0.0617 (3)	0.0091 (2)	0.0388 (2)	0.0631 (2)	0.0121 (1)	0.0597 (2)	0.0125 (2)
	623	4.14499 (1)	0.0587 (3)	0.0065 (2)	0.0356 (2)	0.0603 (2)	0.0098 (1)	0.0571 (2)	0.0094 (2)
0.4	673	4.09170 (1)	0.0665 (3)	0.0151 (3)	0.0406 (2)	0.0671 (3)	0.0179 (3)	0.0530 (3)	0.0240 (3)
0.45	703	4.08266 (1)	0.0616 (3)	0.0092 (2)	0.0345 (2)	0.0616 (2)	0.0118 (2)	0.0459 (2)	0.0189 (2)
0.48	703	4.07677 (1)	0.0616 (3)	0.0099 (3)	0.0360 (2)	0.0611 (3)	0.0120 (3)	0.0459 (3)	0.0206 (3)
0.5	753	4.07469 (1)	0.0611 (3)	0.0099 (3)	0.0360 (2)	0.0607 (3)	0.0121 (3)	0.0457 (3)	0.0209 (3)
0.6	723	4.05409 (1)	0.0552 (3)	0.0006 (4)	0.0318 (1)	0.0570 (3)	0.0029 (4)	0.0406 (2)	0.0175 (3)
1	803	3.96881 (1)	0.0382 (2)	0.0161 (2)	0.0224 (1)	0.0381 (2)	0.0170 (2)	0.0289 (2)	0.0119 (2)

		R_{wp}		R_p		GOF		R_{Bragg}	
x	T (K)	Iso	Aniso	Iso	Aniso	Iso	Aniso	Iso	Aniso
0	523	0.060	0.036	0.039	0.029	2.51	1.50	0.067	0.012
	573	0.058	0.035	0.037	0.028	2.44	1.45	0.065	0.012
0.05	513	0.041	0.024	0.025	0.020	1.67	0.96	0.041	0.008
	573	0.041	0.023	0.026	0.020	1.65	0.94	0.039	0.008
	673	0.039	0.023	0.025	0.020	1.58	0.92	0.039	0.007
0.1	563	0.053	0.028	0.031	0.023	2.00	1.06	0.048	0.009
	623	0.044	0.026	0.029	0.024	2.11	1.26	0.043	0.012
0.4	673	0.034	0.032	0.028	0.027	1.03	0.94	0.016	0.008
0.45	703	0.031	0.027	0.024	0.023	1.21	1.06	0.017	0.007
0.48	703	0.033	0.031	0.027	0.026	1.05	0.98	0.012	0.009
0.5	753	0.031	0.029	0.025	0.024	1.18	1.11	0.012	0.009
0.6	723	0.024	0.023	0.021	0.020	0.86	0.81	0.004	0.004
1	803	0.030	0.028	0.025	0.024	1.09	1.03	0.009	0.010

ISIS (Rutherford Appleton Laboratory) on HRPD (high-resolution powder diffractometer). The samples were packed in 12 mm diameter vanadium canisters. A vacuum furnace with a vanadium heating element was used for the high-temperature measurements. The exposure time for each measurement was around 2.5 h. HRPD experiments were carried out above the Curie temperature according to Jaffe *et al.*'s (1971) original phase diagram for each sample (PZT-0.05 at 513, 573 and 673 K, PZT-0.1 at 563 and 623 K, PZT-0.4 at 673 K, PZT-0.45 at 703 K, PZT-0.48 at 703 K, PZT-0.5 at 753 K, PZT-0.6 at 723 K, $PbTiO_3$ at 803 K and $PbZrO_3$ at 523 and 573 K).

Rietveld refinement was carried out using *TOPAS-Academic* (Coelho, 2005). The data were collected using the high-angle back-scattering bank detectors, which provide the *d*-spacing range ~ 0.3 to 2.2 Å. The scale factor, background parameters, peak-shape function parameters and absorption parameters were refined in all cases.

3. Results and discussion

A model in the space group $Pm\bar{3}m$ with isotropic displacement parameters for oxygen was examined first for all the compositions. This model provided small *R* factors, but close examination of the observed and calculated peak profiles revealed significant discrepancies (Fig. 1). For {211}, {311}, {004}, {322}, {033}, {421}, {043} ... peaks, the observed intensity was higher than calculated; for {031}, {032}, {332}, {432}, {521}, {006} ... peaks, it was lower. With increasing x the intensities of these particular reflections became smaller. The discrepancies obviously did not follow any systematic trend and inclusion of the Pb disorder model of Kuroiwa *et al.* did not help to improve the fits.

We therefore considered the possibility that the O atoms might be statistically disordered about their average positions at ($\frac{1}{2}$,0,0), (0,$\frac{1}{2}$,0) and (0,0,$\frac{1}{2}$) by displacing them through a small distance u to give ($\frac{1}{2}$,u,0), (0,$\frac{1}{2}$,u) and (u,0,$\frac{1}{2}$) (making ⟨100⟩ displacements) or ($\frac{1}{2}$,u,u), (u,$\frac{1}{2}$,u) and (u,u,$\frac{1}{2}$) (making ⟨110⟩ displacements). This definitely greatly improved the fit to the data. However, the best fit was obtained by introducing refinement of the anisotropic displacement parameters for the O atom (set at 0,0,$\frac{1}{2}$: $U^{11} = U^{22} \neq U^{33}$, $U^{12} = U^{13} = U^{23} = 0$, and equivalent relationships for the other special oxygen positions) to the ordered cubic model (Fig. 1), especially for compounds whose compositions were on the Zr-rich side of the MPB. R_{Bragg} is a good indicator of agreement in a cubic material (Table 1) and it is seen that with the introduction of oxygen anisotropy it decreases dramatically for low Ti content but that for the end-member $PbTiO_3$ there is hardly any change. This indicates that as the Ti content increases, the anisotropic model becomes less relevant, until for $PbTiO_3$ an isotropic model is perfectly adequate (this is not surprising

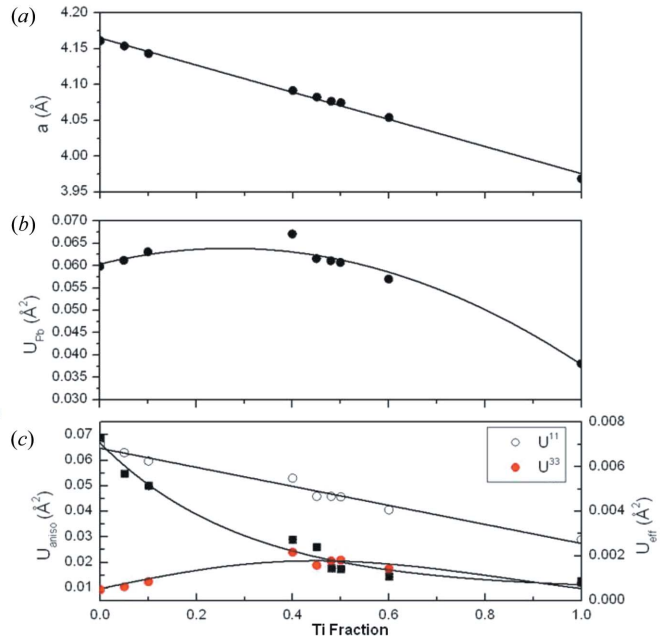

Figure 2
Structural parameters as a function of Ti content. (*a*) Lattice parameter; (*b*) isotropic displacement parameter for Pb; (*c*) for O-atom U^{11} (open circles); U^{33} (filled circles); $U_{\rm eff}$ (filled squares).

given that $PbTiO_3$ has always been considered to have a fully ordered perovskite structure). This trend can also be seen by plotting the quantity

$$U_{\rm eff} = (2U^{11} + U^{33})/3 - U_{\rm iso} \qquad (1)$$

for the O atom against Ti content (Fig. 2). This shows that the oxygen ellipsoid is flattened on the {001} planes at all compositions, and this flattening is most severe in the Zr-rich region. The variation of $U_{\rm eff}$ indicates a decrease of the octahedral tilting disorder with increasing Ti concentration.

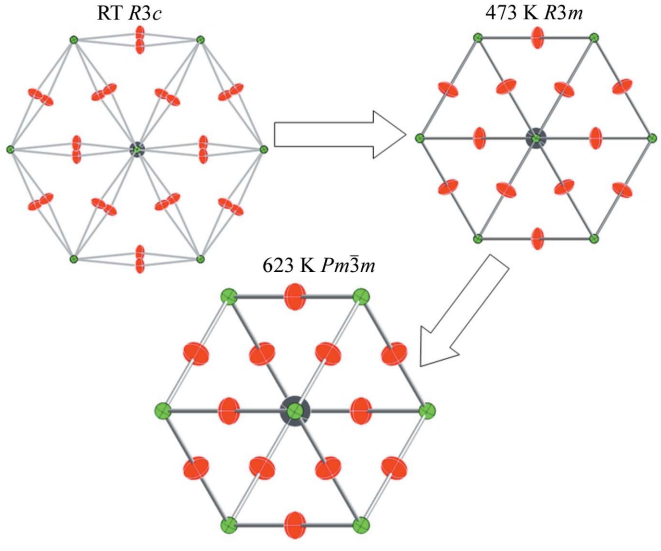

Figure 3
Plot of the PZT-0.1 structures at 300, 473 and 623 K projected down the threefold axis.

This is corroborated by the observation that the intensities for most of the peaks that are not well fit by the isotropic model ({211}, {311} *etc*) decrease in the Ti-rich region and finally become zero in the $PbTiO_3$ powder diffraction pattern.

Note that for pure $PbZrO_3$ some extra peaks were present in the pattern, which were determined to arise from unreacted ZrO_2. This was included in the Rietveld refinement as a second phase.

A plot of the PZT-0.1 structure at 623 K projected on (111) (Fig. 3) shows that the oxygen ellipsoids are reminiscent of the octahedral tilting seen in the lower-symmetry room-temperature *R*3*c* phase. Furthermore, the 473 K structure shows the same effect in *R*3*m* symmetry, which has no long-range tilts, as indicated by the absence of $a^-a^-a^-$ tilt reflections. Note that Glazer, Mabud & Clarke refined the *R*3*m* structure using the PZT-0.1 data as long ago as 1978 and commented on the possibility of oxygen disorder. Our refinements show that with increasing temperature, rhombohedral PZT loses its long-range octahedral tilting at the *R*3*c*–*R*3*m* transition with the tilting of the oxygen octahedra becoming disordered about [111]. The present work shows that this tilt disorder persists beyond this phase transition *even* into the high-temperature cubic phase. It is interesting to note in this context that recent anelastic and dielectric experiments on PZT-0.1 by Cordero *et al.* (2011) have found a diffuse phase transition above the *R*3*c*–*R*3*m* transition that they propose heralds the appearance of short-range octahedral tilts within the *R*3*m* phase.

Our work shows some substantial differences from the results of Kuroiwa *et al.* In their case when refined anisotropically, they obtained flattened oxygen ellipsoids (their Fig. 1) similar to ours and as with our results, the ellipsoids tended to become more isotropic with increasing Ti content.

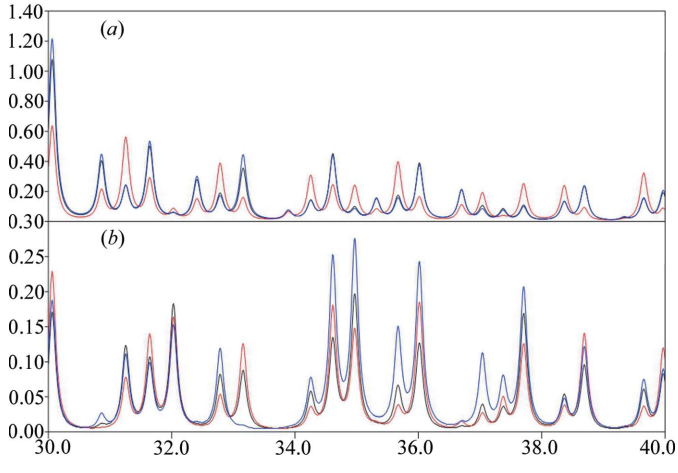

Figure 4
(*a*) X-ray and (*b*) neutron angle-dispersive powder diffraction simulations (Crystallographica, Oxford Cryosystems, Ltd) for pure $PbZrO_3$. The angular range shown corresponds approximately to that shown by Aoyagi *et al.* (2002) and by Kuroiwa *et al.* (2005) in which the sensitivity to small structural parameter changes was high. Black: model 1 – all atoms isotropic; red: model 2 – Pb atoms disordered along ⟨110⟩; blue: model 3 – anisotropic O atoms.

However, when they included Pb disorder the anisotropy of the oxygen ellipsoids remained largely independent of Ti content (their Table II).

In order to understand this difference we calculated (Fig. 4) the angle-dispersive X-ray and neutron powder patterns for cubic $PbZrO_3$ at a wavelength of 0.36 Å for three cases:

(1) all atoms isotropic and ordered;

(2) Pb atoms disordered along ⟨110⟩, O and Zr ordered, all atoms isotropic (model of Aoyagi *et al.*, 2002);

(3) anisotropic displacement parameters for the O atoms and all atoms ordered (our model in the present work).

The neutron diffraction simulations showed that model 3 is easily distinguishable, whereas models 1 and 2 give patterns that are less easily distinguished from each other, even at the low angles at which the highest intensity peaks occur in the diffraction patterns. By contrast, the X-ray diffraction simulations for models 1 and 3 are very similar, but model 2 can be readily distinguished. Thus, the X-ray measurements are not sufficiently sensitive to determine the oxygen disorder unequivocally, but are rather dominated by the effect of disordered Pb. With neutron diffraction, however, we have been able to make a definitive choice of model 3 (anisotropic O atoms) over model 2 (disordered Pb atoms), something that could not have been achieved using X-ray data alone.

Finally, to determine whether any Pb disorder might also be present, nonetheless, we plotted difference-Fourier maps around the Pb and O atoms for model 3 for $PbZrO_3$ and for PZT-0.1 (Fig. 5). In pure $PbZrO_3$ there is some evidence of ⟨110⟩ displacements for Pb, in agreement with Aoyagi *et al.* Similarly the O-atom map indicates ⟨110⟩ displacements, although the map is complicated by some extra residual density further out along ⟨310⟩ approximately. On the other hand, the difference map for PZT-0.1 seems to indicate mainly ⟨100⟩ disorder for the Pb atom, rather than along ⟨111⟩ as was suggested by Kuroiwa *et al.*. When ⟨100⟩ Pb displacements were included in the neutron Rietveld refinement of PZT-0.1, $R_{\rm Bragg}$ was further reduced from 1.21 to 1.08%, in good agreement with the evidence seen in the difference-Fourier map. All other types of Pb displacement led to larger values of $R_{\rm Bragg}$. Furthermore, the difference-Fourier map for the oxygen shows evidence of statistical disorder along ⟨100⟩ and ⟨110⟩, consistent with the flat anisotropic ellipsoid of model 3. However, with increasing Ti the apparent disorder becomes less directionally defined and so we conclude that in PZT, especially for the Zr-rich compositions, it is oxygen octahedral disorder that is the primary feature of interest, coupled possibly with some Pb disorder.

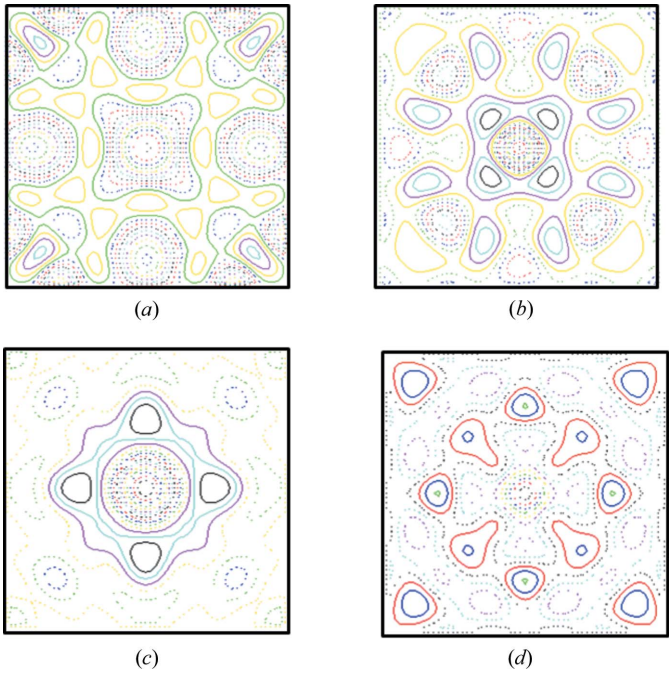

Figure 5
Difference-Fourier map viewed down [001] after anisotropic refinement of the O atoms. Distance across each map 1.6 Å. (*a*) $PbZrO_3$ Pb atom; (*b*) $PbZrO_3$ O atom at $(0,0,\frac{1}{2})$; (*c*) PZT-0.1 Pb atom; (*d*) PZT-0.1 O atom at $(0,0,\frac{1}{2})$.

4. Conclusions

Rietveld refinements using high-resolution neutron time-of-flight data for the cubic phase of PZT show anisotropic displacement ellipsoids for the O atoms that are consistent with the presence of disordered octahedral tilting. This disorder can be thought as (*a*) either a remnant of the long-range tilting seen in the room-temperature *R*3*c* phase on heating or (*b*) the precursor to the same on cooling. This feature exists over the whole compositional range, but is most pronounced in the Zr-rich region. It should be noted that it is not possible at this stage to decide whether this disordering is dynamic (thermal) or static in origin. However, the shape of the anisotropic displacement ellipsoid for the O atom is consistent with the symmetry-adapted vectors for R_4^+ or M_3^+ phonon modes, which when condensed lead to long-range − or + tilting. As the lower-temperature *R*3*c* phase involves $a^-a^-a^-$ tilts, it is likely that it is the R_4^+ mode that is active here. To verify this, additional structural work at variable temperatures within the cubic phase is required. In addition, we shall be carrying out PDF analysis of these ceramics in the near future in order to complement the present study. Our present work further suggests that in general careful structural studies of the largely ignored cubic perovskite phases are imperative to the understanding of the distorted non-cubic phases, which are of importance for technological applications. Far from being simple cubic structures, they present a degree of complexity that has hitherto been overlooked by all but a few researchers. In our opinion this work points towards a rich field of study within these high-symmetry phases that is amenable to attack both by further experiment and theory.

This work was funded by the EPSRC-NSF (Materials World Network: Nanoscale Structure–Property Relationships in Lead-free Morphotropic Phase Boundary Piezoelectrics). We are grateful to the Rutherford-Appleton Laboratory for access to the ISIS HRPD diffractometer.

References

Aoyagi, S., Kuroiwa, Y., Sawada, A., Tanaka, H., Harada, J., Nishibori, E., Takata, M. & Sakata, M. (2002). *J. Phys. Soc. Jpn*, **71**, 2353–2356.

Clarke, R. & Glazer, A. M. (1974). *J. Phys. C*, **7**, 2147–2156.

Coelho, A. A. (2005). *J. Appl. Cryst.* **38**, 455–461.

Cordero, F., Trequattrini, F., Craciun, F. & Galassi, C. (2011). *J. Phys. Condens. Matter*, **23**, 415901.

Corker, D. L., Glazer, A. M., Whatmore, R. W., Stallard, A. & Fauth, F. (1998). *J. Phys. Condens. Matter*, **10**, 6251–6269.

Glazer, A. M. (1972). *Acta Cryst.* B**28**, 3384–3392.

Glazer, A. M., Mabud, S. A. & Clarke, R. (1978). *Acta Cryst.* B**34**, 1060–1065.

Glazer, A. M., Thomas, P. A., Baba-Kishi, K. Z., Pang, G. K. H. & Tai, C. W. (2004). *Phys. Rev. B*, **70**, 184123, 1–9.

Jaffe, B., Cook, W. R. & Jaffe, H. (1971). *Piezoelectric Ceramics*. New York: Academic Press.

Kuroiwa, Y., Terado, Y., Kim, S. J., Sawada, A., Yamamura, Y., Aoyagi, S., Nishibori, E., Sakata, M. & Takata, M. (2005). *Jpn. J. Appl. Phys.* **44**, 7151–7155.

Noheda, B., Cox, D. E., Shirane, G., Gonzalo, J. A., Cross, L. E. & Park, S.-E. (1999). *Appl. Phys. Lett.* **74**, 2059–2061.

Welberry, T. R., Baba-Kishi, K. Z. & Withers, R. L. (2010). *Key Eng. Mater.* **421–422**, 389–394.

Whatmore, R. W., Clarke, R. & Glazer, A. M. (1978). *J. Phys. C*, **11**, 3089–3102.

Yokota, H., Zhang, N., Taylor, A. E., Thomas, P. A. & Glazer, A. M. (2009). *Phys. Rev. B*, **80**, 104109.

Zhang, N., Yokota, H., Glazer, A. M. & Thomas, P. A. (2011). *Acta Cryst.* B**67**, 386–398.